SERGEY BRAGIN[1]
JOSEF WATZINGER[1]
BERND LINZER[1]
ANDREA BIANCHI[2]
CHRISTIAN BERNHARD[3]

INFLUENCE OF THIN SLAB THICKNESS ON FINAL STRIP PROPERTY IN ARVEDI ESP PLANT

Abstract

Application of thin slab direct rolling (TSDR) technology became widespread in the last decades. This technology occupied a corresponding niche in the strip production through its continuous development in productivity and product quality.

The Arvedi Endless Strip Production (ESP) Technology was put into operation in 2009. The plant consists of single thin slab caster directly connected to three-stand high reduction mill and a five-stand finishing mill after temperature adjustment in an inductive heating unit. The Arvedi ESP plant became one of the most productive thin slab casting plants in the world shortly after starting up. The production capacity for an ESP line is up to 2.6 Mt/a for certain product mix, based on actual production figures.

The ESP caster is equipped with either a 110 or 90mm thick funnel shaped mould and liquid core reduction. The ESP caster is designed to allow a very high flexibility in strand thicknesses being fed into the first rolling step. This is utilized by Arvedi by producing typical strand thickness of 80 to 100 mm. Comparing different casting thicknesses at the same mass flow results in different casting speeds and rolling schedules. The present work describes the influence of slab thickness and casting speed on slab quality and microstructure evolution in the production of micro alloyed steel strips at the Arvedi ESP plant.

[1] Siemens VAI, Linz, Austria
[2] Acciaieria Arvedi Spa, Cremona, Italy
[3] Leoben University, Leoben, Austria

1 Introduction

Thin slab casting is a key point within this technology as it defines the productivity as well as the preconditions for the forthcoming rolling steps.

The Arvedi Endless Strip Production (Arvedi ESP) line is the first representative of the endless TSCR process that yielded 2.0 mio.t in 2013 on a single strand. Design of ESP caster is optimised for high mass flow. Special Arvedi mould geometry provides slab thickness of 110 or 90 mm prior to liquid core reduction. A bow-type caster has been designed with liquid core bending and straightening, keeping the ferrostatic pressure very low. This approach assures constant and high casting speed i.e. mass flow. The typical slab thickness is 80-100 mm.

The production of this process shows outstanding production stability (reflected e.g. in lowest break out rates) and product quality results the highest casting speed in the area below 6 m/min. By further increase of the specific productivity, and therefore raising of the casting speeds certain technical limits are expected, which can be found e.g. at the system tundish-submerged entry nozzle (SEN)-mould and strains that are accumulated in solidification front caused by bulging and bending/straightening of the slab. Casting speeds of up to 7 m/min are in the design range of a typical ESP line. Higher casting speeds of up to 8 m/min reported elsewhere [1, 2], which proves the basic operation possibility of casters at such conditions, without mentioning of the influence to process stability, availability and yield by using current available materials and solutions at the mould area.

At constant capacity the proportion of casting speed and slab thickness can be varied. In endless operation, these parameters define the distribution of temperature, strain and strain rate through the slab thickness in high reduction mill as well as interpass time. Therefore, the microstructure evolution during casting and rolling is strictly dependent on casting parameters.

The present study uses the computer simulation for analysis of comparable mass flows by different combination of casting speeds and slab thicknesses and the given influence to slab quality and microstructure evolution during casting and rolling. The process parameters and chemical composition for the analysis are specified in **Fig. 1** and **Table 1**. The thickness of transfer bar in all cases is 16 mm and final strip thickness is 2,5 mm.

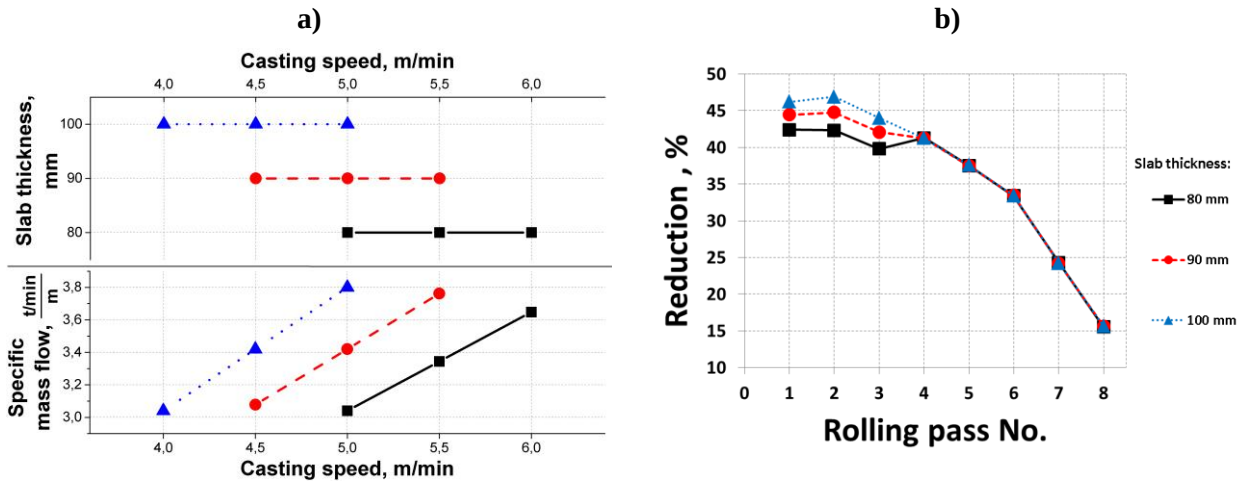

Fig. 1: Plan for analysis: a) casting parameters; b) rolling schedules

Table 1: Chemical composition of S360

Weight %					
C	Si	Mn	Al	Nb	N
0,04-0,06	0,15-0,25	0,45-0,55	0,025-0,035	0,02-0,03	0,005-0,008

2 Characteristic of thin slab

Temperature distribution through the slab thickness

Addition to conventional casting strategies, at TSCR it is on major motivation to save energy by exploiting the thermal heat of cast slab. In case of the ESP process it is even realized to directly roll on the slab without any heating facility between the casting and rolling steps. For this configuration the so called inverse temperature profile is present at the first rolling step. That means, that the slab, having a hot core and undercooled surface coming from casting is rolled within the first rolling step.

This temperature profile is invers to common slabs after coming from reheating furnaces, which are hotter at the surface due to heat introduction at the centre of the slabs by conductivity from the surface. The metallurgical length of a typical ESP caster is 18,5 m and consists of 8 cooling zones, which allows good control of surface temperature and solidification. **Fig. 2** shows the result of solidification simulation. The material data for simulation was prepared using IDS16 [3] software and the solidification simulation was carried out using a transient FV-model in one dimension [24]. The increase of slab thickness and casting speed increases temperature differences between slab surface and centre, which is between 200 and 340°C for considered casting parameters.

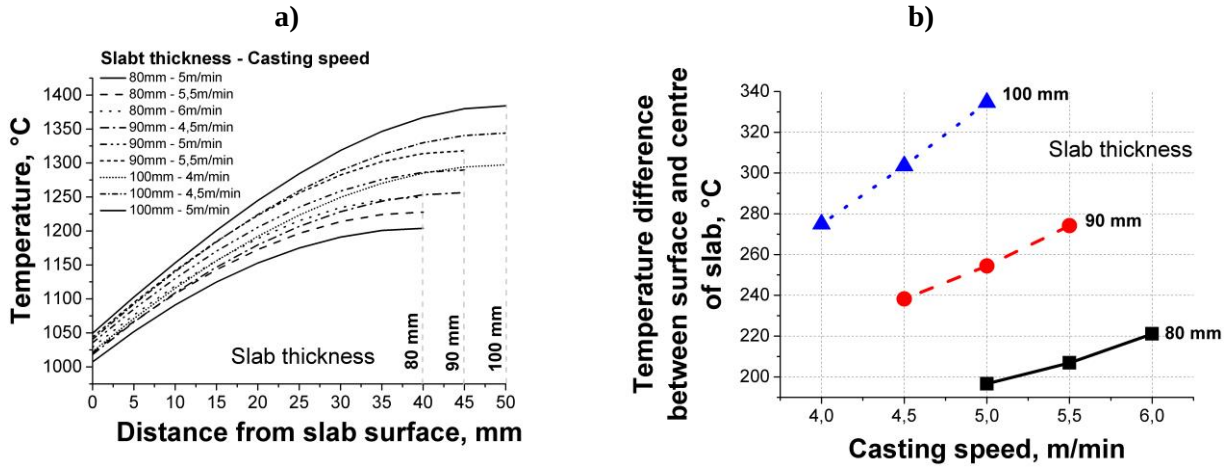

Fig. 2: a) Temperature profile of thin slab and b) temperature difference between slab surface and centre at the exit of continuous casting machine

Primary microstructure

The solidification simulation shows that the local solidification conditions are very similar for all considered cases. The local solidification time (LST) is the time spent within the two phase region (liquid-solid) required for full solidification of a representative volume, coming from total liquid (solid fraction 0) at liquidus temperature to full solidified status (solid fraction 1) at solidus temperature (**Fig. 3a**). The evolution of LST through the slab thickness is given in **Fig. 3b**. Since the secondary-dendrite-arm-spacing (SDAS) is the function of LST, the primary

microstructure is also very similar for all considered cases (**Fig. 3b**). Only the maxima SDAS in slab centre is different for various slab thickness. SDAS was calculated using the following equations and coefficients proposed by *Pierer & Bernhard (2008)* [4]:

$$SDAS = K \cdot LST^{n}$$

$$K = 23{,}7 - 13{,}1 \cdot (gw.\%C)^{\frac{1}{3}} \; ; \; n = \frac{1}{3} \tag{1}$$

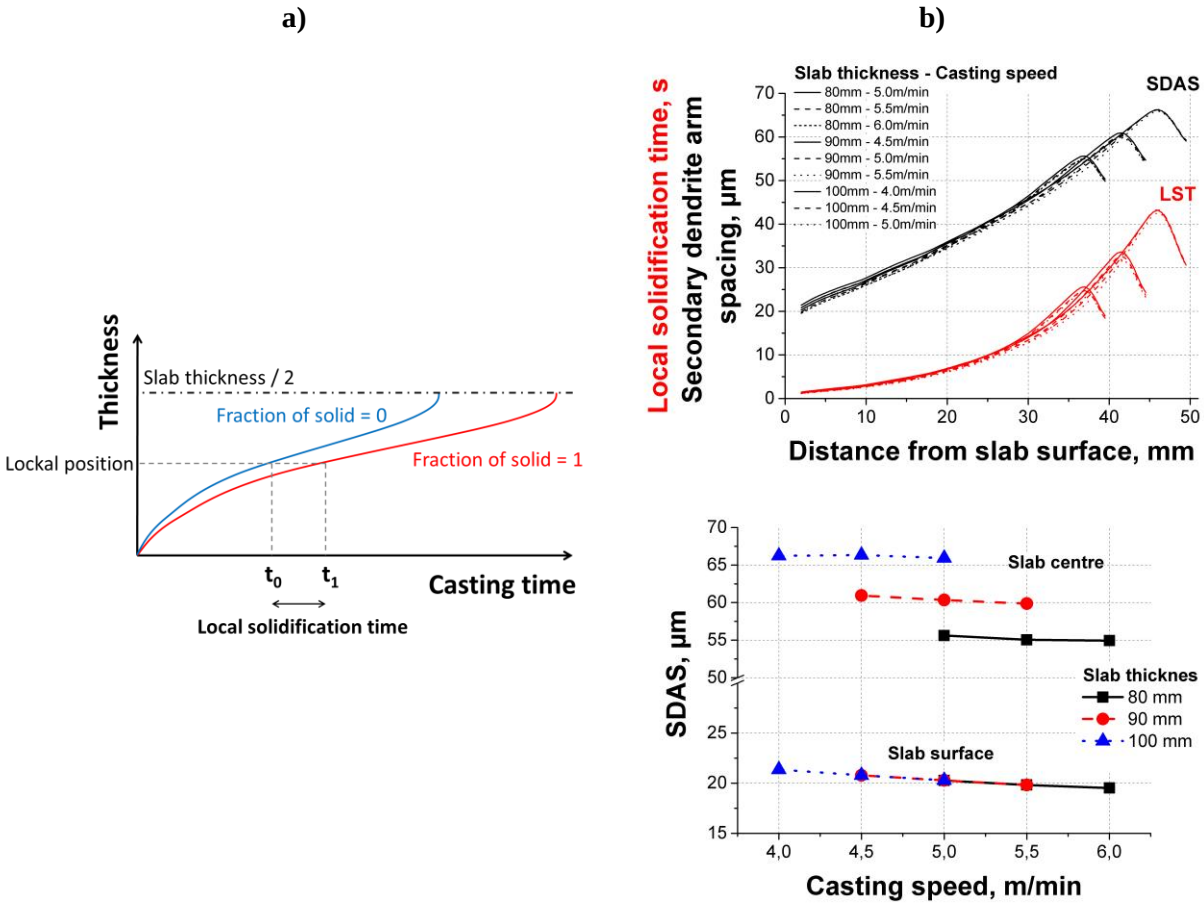

Fig. 3: a) Definition of local solidification time; b) Local solidification time calculated with Sol-A-Sys and secondary dendrite arm spacing calculated with Eq.1

Micro-segregation

S360 is a micro-alloyed steel with low carbon content. The interdendritic enrichment of alloying elements for this steel is typically very low. The micro-segregation was calculated for interdendritic solidification between secondary dendrites (**Fig. 4a**). The solidification starts with the formation of ferrite. During solidification the retained liquid is enriched with Nb and Mn. Al depletes the retained liquid due to the different character of distribution between liquid and solid. The arisen enriched and depleted regions are homogenised in ferrite region after solidification through diffusion phenomena. The diffusion in single phase is described by Fick's second law:

$$\frac{\partial c}{\partial t} = D \cdot \frac{\partial^2 c}{\partial x^2}$$	(2)
C - concentration, $\frac{mol}{m^2}$; D - diffusion coefficient, $\frac{m^2}{s}$; t – time, s; x – position, m	

By ferrite-austenite transformation the Mn diffuses into austenite since higher solubility. On the other hand, Nb and Al remain in ferrite till the end of transformation. The homogenisation of enriched areas happens after transformation. This process is controlled by diffusion and is calculated by Fick's second law (Eq.2).

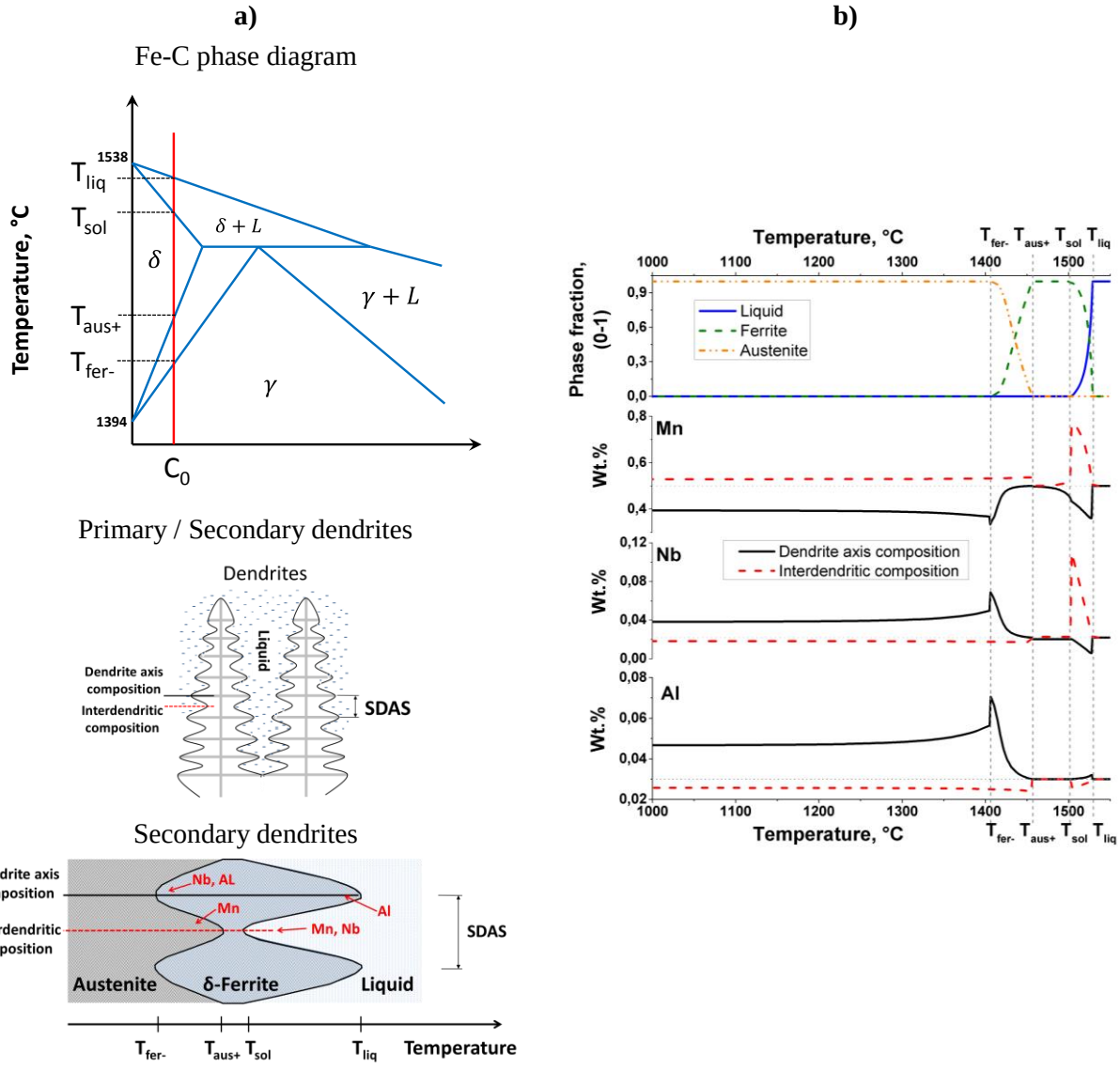

Fig. 4: a) Fe-C Phase diagram and schematic illustration of various stages of micro-segregation during solidification; b) Dendrite axis composition and interdendritic composition for surface of 100 mm slab, 5 m/min casting speed

Fig. 4b shows the phase transformation and evolution of composition for dendrite axis and interdendritic area. The micro-segregation was calculated using IDS16 software [3] on the basis of SDAS from **Fig. 3** and cooling lines from solidification simulation. The approach for micro-segregation calculation [12] assumes the complete solute mixing in liquid and finite difference application for diffusion in single phase regions. The formation of MnS in region Liquid + δ-Ferrite is also taken into micro-segregation calculation. **Fig. 5** shows the micro-segregation index of Mn, Nb and Al through slab-thickness at the exit of continuous casting machine. The maximal deviation of micro-segregation index is in areas with hindered diffusion due to deceleration at low temperature in subsurface area or long diffusion paths (SDAS) in slab centre. Segregation index of considered elements is marginally dependent on casting speed and slab thickness.

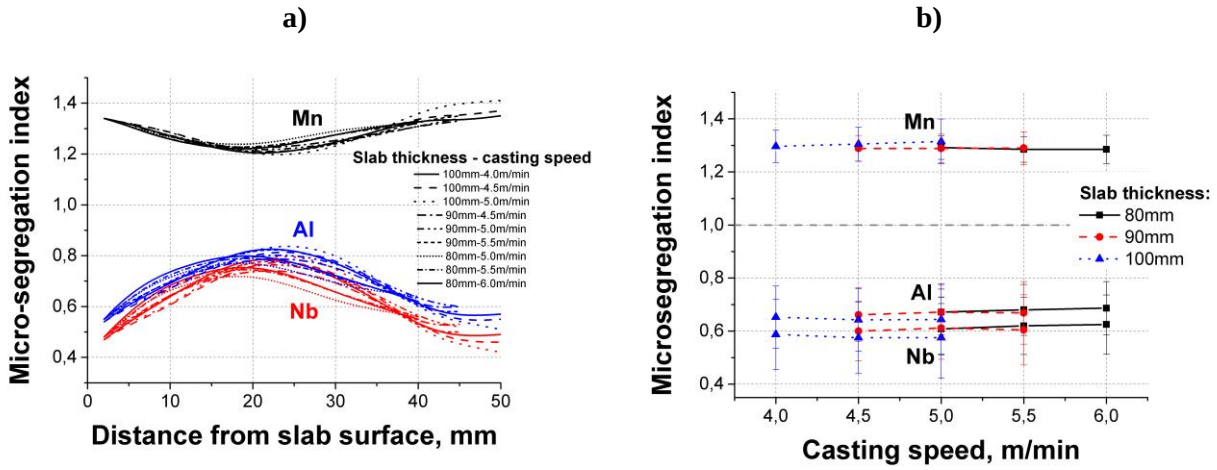

Fig. 5: a) Micro-segregation of manganese, niobium and aluminium as function of distance to slab surface, (micro-segregation index = interdendritic composition/dendrite axis composition); b) mean micro-segregation index

Precipitations

Nb(C,N) and AlN are the possible precipitations for S360. According to thermodynamic equilibrium calculation, the subsurface temperature is below onset of Nb(C,N) and AlN [13]. Software MatCalc [5] was used for precipitation calculation. MatCalc includes modules for describing both, equilibrium thermodynamics as well as kinetics/diffusion of precipitation nucleation and growth. Dislocations and grain boundaries were considered as nucleation sites for precipitation. **Fig. 6** presents the surface temperature and the time-temperature-precipitation (TTP) diagrams of Nb(C,N) and AlN for dendritic axis composition. The precipitation calculation shows that onset of precipitations (>0,1% phase fraction) does not take place during continuous casting for all considered slabs and the precipitation has negligible impact on austenite grain growth and ductile properties.

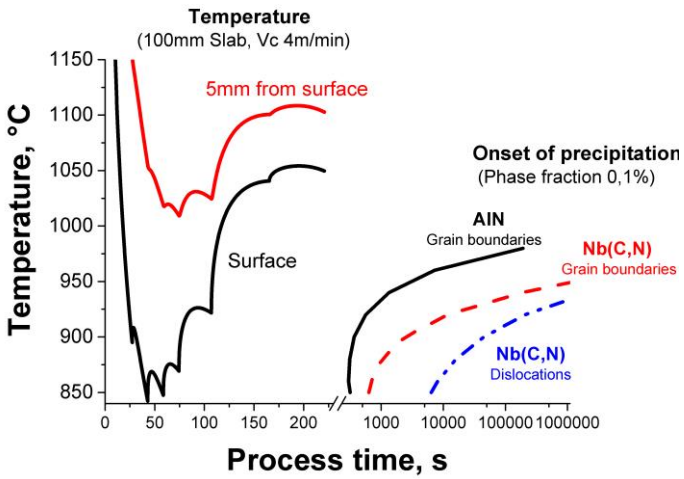

Fig. 6: Onset of AlN and Nb(C,N) on the slab surface in interdendritic area for 100 mm slab, 4 m/min

Austenite grain size

The austenite grain growth during continuous casting was calculated by using model (**Tab. 3 - Eq. 6**) and coefficients like activation energy that were proposed by *Andersen & Grong* (1995) [6] and *Bernhard et.al.* (2008) [7]. **Fig. 7a** shows the calculated distribution of austenite grain size through the slab thickness at the exit of continuous casting machine. The grain growth rate is strongly dependent on temperature and time. Therefore, the fast cooling to the low temperatures leads to hindered grain growth at the subsurface area.

The temperature in next layers from slab surface becomes higher and the grain growth is more intensive.

But the time for grain growth get shorter hence the grain size in the slab centre is smaller than in ¼ of the slab thickness. This grain size distribution is used as initial condition for microstructure evolution in rolling part. The decrease of casting speed and increase of slab thickness lead to an increase of the average austenite grain size from 1280 µm to 1440 µm (**Fig. 7b**). An influence of casting speed on austenite grain size is more pronounced for thicker slabs.

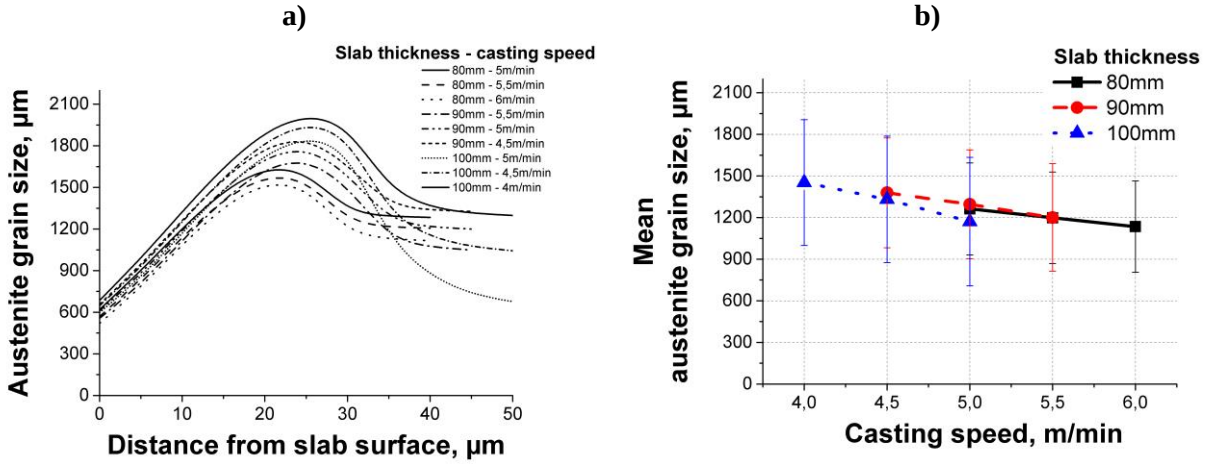

Fig. 7: a) Austenite grain size as function of distance to slab surface; b) Mean austenite grain size with standard deviation as function of casting speed

Internal quality

The bow type caster achieves a decrease of ferrostatic pressure. The tensile strain on the solidification front, which is caused by bulging and straightening, can be estimated using the following empirical equations:

Table 2: Model for estimation of internal cracking

Model	Eq.	References
$\varepsilon_{bulging}\,[\%] = \frac{1600 \cdot s \cdot y_{max}}{L^2} \cdot 100$	(3)	[8]
$y_{max}\,[\mathrm{mm}] = 7{,}86 \cdot 10^{-12} \cdot exp(0{,}0046 \cdot T) \cdot \frac{L^{6,1} \cdot H^{2,25}}{v^{0,57} \cdot s^{5,26}}$	(4)	[9]
$\varepsilon_{straightening}\,[\%] = \left(\frac{d}{2} - s\right) \cdot \left(\frac{1}{R_{n-1}} - \frac{1}{R_n}\right) \cdot 100$	(5)	[10]

d – slab thickness, mm	s – shell thickness, mm
H – height from meniscus, m	T – temperature, K
L – roll pitch, mm	v – casting speed, m/min
R_{n-1} , R_n– radii of roll number $n-1$ and n, mm	y_{max} – bulging, mm

Strain accumulation between 0.96 and 1 fraction of solid was assumed for this calculation. **Fig. 8** shows the distribution of accumulated strain through the slab thickness. Increasing the slab thickness results in various effects on strain accumulation which are mainly caused by bulging or straightening. The strain caused by bulging becomes smaller and the strain caused by straightening becomes bigger (**Fig. 8a**). The increase of casting speed leads to an increase of strain caused by both bulging and straightening s. **Fig. 8b**. For this steel grade, the critical strain for formation of internal cracks is > 0,5% [11]. The accumulated strain of the considered slab amounts to less than 0.25% that ensures the excellent internal quality of the slab.

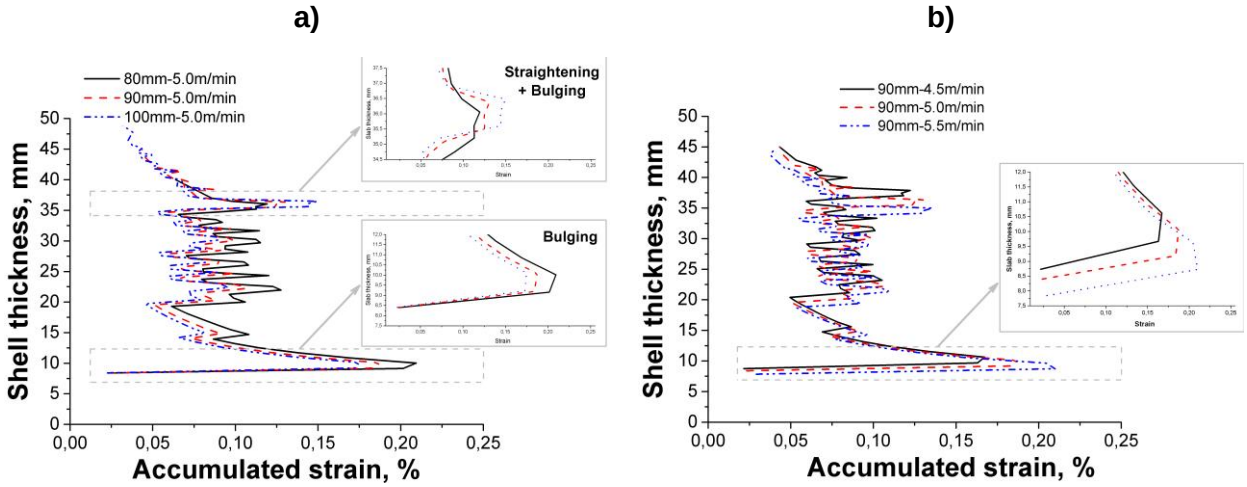

Fig. 8: Accumulated strain in solidification front. a) Influence of slab thickness; b) Influence of casting speed

3 Characteristic of hot rolled strip

Microstructure modelling

Table 3 summarises the microstructure model equations used for description of the grain size evolution during continuous casting, hot rolling and cooling. The model for the rolling part considers the austenite evolution during deformation and softening due to recrystallization and grain growth at interpass times. Microstructure calculation is coupled with precipitation simulation (Software MatCalc [5]) proceed simultaneously by cyclic data exchange. The microstructure model provides grain size and dislocation density and the precipitation model provides the amount of precipitation to predict the start of strain accumulation due to the pinning effect of Nb(C,N) after deformation.

Both, thermally induced as well as strain induced precipitation were taken into account in the precipitation model. It was assumed that pipe diffusion increases immediately during austenite deformation because of increasing dislocation density. Moreover, it was assumed that the volumetric misfit between steel matrix and precipitates can be neglected. Both assumptions lead to a significant overestimation of the speed of precipitation kinetics.

Tab. 3: Microstructure model

Phenomenon	Model	Eq.	References
Grain growth for as-cast microstructure	$\frac{dd}{dt} = M_0^* \cdot \exp\left(-\frac{Q_{app}}{R \cdot T}\right) \cdot \left(\frac{1}{d} - \frac{1}{k_Z} \cdot \frac{f}{r}\right)^{\left(\frac{z}{n-1}\right)}$ $Q_{app} = 167686 + 40562 \cdot C_p$ $C_p = Wt.\%C - 0{,}14 \cdot Wt.\%Si + 0{,}04 \cdot Wt.\%Mn$	(6)	[6, 7]
Peak strain Critical strain for DRX / MDRX	$\varepsilon_p = 0{,}0037 \cdot \frac{1 + 20 \cdot Wt.\%Nb}{1{,}78} \cdot D^{0{,}147} \cdot \left(\dot{\varepsilon} \cdot \exp\left(\frac{325000}{R \cdot T}\right)\right)^{0{,}155}$ $\varepsilon_c = 0{,}8 \cdot \varepsilon_p$	(7)	[14]
DRX	$X = 1 - \exp\left(-0.693 \cdot \left[\frac{\varepsilon - \varepsilon_c}{\varepsilon_{0,5} - \varepsilon_c}\right]^2\right)$ $\varepsilon_{0,5} = 0{,}001144 \cdot D^{0{,}28} \cdot \dot{\varepsilon}^{0{,}05} \cdot \exp\left(\frac{51880}{R \cdot T}\right)$	(8)	[15]
MDRX	$X = 1 - \exp\left(-0.693 \cdot \left[\frac{t}{t_{0,5}}\right]^2\right)$; $t_{0,5} = \frac{1{,}77 \cdot 10^{-6}}{\dot{\varepsilon}^{0{,}62}} \cdot \exp\left(\frac{152000}{R \cdot T}\right)$ $D_{RX} = 1370 \cdot \dot{\varepsilon} \cdot \exp\left(\frac{375000}{R \cdot T}\right)^{-0{,}12}$	(9)	[16, 17]
SRX	$X = 1 - \exp\left(-0.693 \cdot \left[\frac{t}{t_{0,5}}\right]^1\right)$ $t_{0,5} = \frac{9{,}92 \cdot 10^{-11} \cdot \exp\left[\left(\frac{275000}{T} - 185\right) \cdot Wt.\%Nb\right] \cdot D_0}{\varepsilon^{5,6 \cdot D_0^{-0,12}} \cdot \dot{\varepsilon}^{0,52}} \cdot \exp\left(\frac{180000}{R \cdot T}\right)$ $D_{RX} = 1{,}4 \cdot D_0^{0{,}56} \cdot \varepsilon^{-1}$	(10)	[18, 19]
Grain growth for interpass time	if $X \geq 0{,}9$ $D^{4,5} = D_{RX}^{4,5} + 4{,}1 \cdot 10^{22} \cdot t \cdot \exp\left(-\frac{435000}{R \cdot T}\right)$	(11)	[20]
Effective strain	$\varepsilon_{eff} = \varepsilon_i + \lambda \cdot (1 + X_{i-1}) \cdot \varepsilon_i$ $\lambda = 1$ if $X < 0{,}1$ and $\lambda = 0{,}5$ if $X \geq 0{,}1$	(12)	[21]

Ferrite grain size	$D_a^* = 4{,}5 + \frac{3}{\sqrt{\dot{T}}} + 13{,}4 \cdot (1 - \exp(-0{,}015 \cdot D_0))$ $D_a = D_a^* \cdot (1 - 0{,}5 \cdot \varepsilon_{eff}^{0{,}47})$	(13)	[22]

D – Grain size, µm ; d – Grain size, m f – volume fraction of precipitates k_Z – Zener coefficient M_0^* - physical constant related to the grain boundary mobility n – time exponent R - universal gas constant, $8{,}314\ ^{J}/_{(mol \cdot K)}$	r – radius of precipitates, m T – Temperature, K t – time, s ε – strain $\dot{\varepsilon}$ – strain rate, $^{1}/_{s}$ $\dot{T}$ – cooling rate, $^{K}/_{s}$

Microstructure evolution during hot rolling

The microstructure simulation was carried out for strip surface, ¼ strip thickness and strip core. The temperature profiles were calculated with internal software of Siemens VAI. The homogeneous strain distribution through the strip thickness is assumed for this microstructure simulation.

Fig. 9 shows the temperature and results of microstructure simulation for thin slab thickness of 90 mm and casting speed of 5 m/min. The coarse as-cast austenite grains are significantly refined in the high reduction mill due to dynamic and static recrystallization. Between high reduction and finishing mill growing austenite grains are observed, especially during inductive heating. **Fig. 10a** represents the austenite grain size prior to induction heating for different casting speeds and slab thicknesses. The increase of casting speed and slab thickness leads to bigger austenite grain size through the slab thickness. After induction heating the austenite grain size is homogenised through the strip thickness and is between 80 and 90 µm for all considered cases. Rolling in the finishing mill occurs partially below the non-recrystallization temperature. The microstructure is fully recrystallized after the first two passes. During the subsequent passes strain accumulation and pancaking occurs. The influence of casting speed and slab thickness on austenite grain size and accumulated strain isn't observed at finishing mill exit. The final austenite grain size is 17,5-19 µm on the strip surface and 19,4-21,4 µm in centre of the strip for all considered cases. The strain accumulation after last rolling pass is around 0,71.

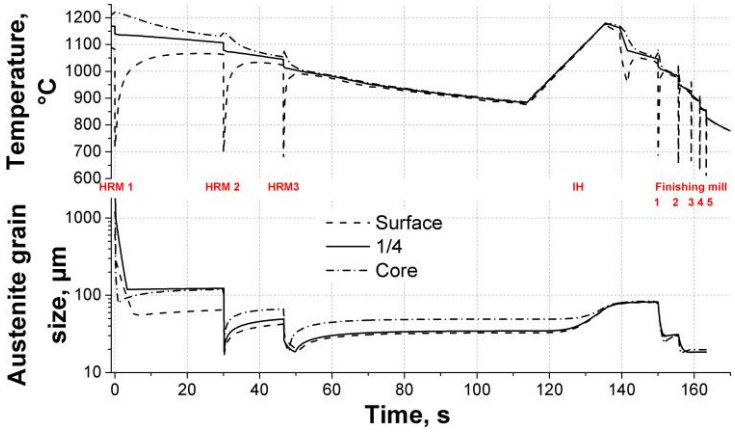

Fig. 9: The results of the microstructure simulation for 90 mm 5 m/min

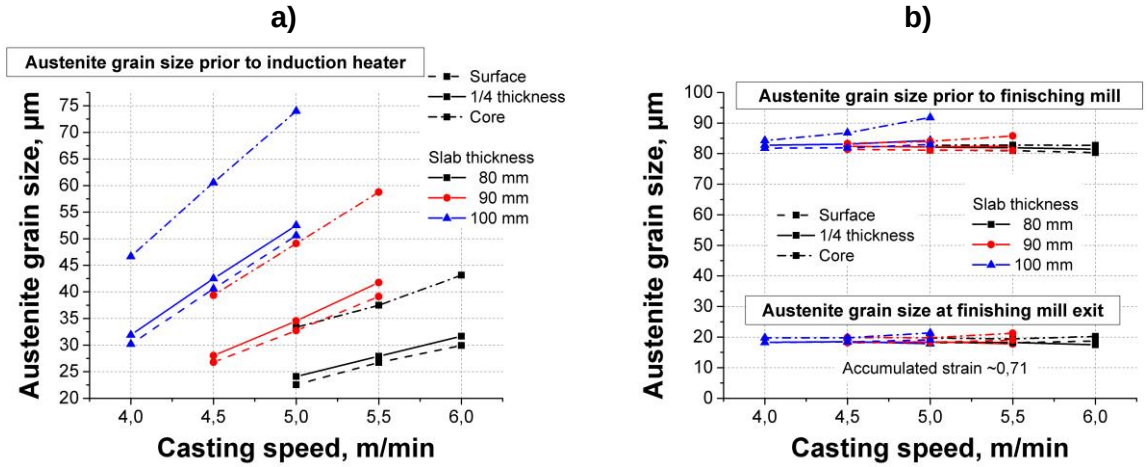

Fig. 10: Austenite grain size a) prior to induction heating; b) at finishing mill entry and exit side

Fig. 11a and b shows the final ferrite grain size and strengthening effect of ferrite grain calculated with Hall-Petch relationship with coefficient of 15,1 [23] for different cooling rates in cooling line. The grey areas display the austenite grain size on strip surface, ¼ strip thickness and strip core. It illustrates that the influence of casting parameters on final microstructure and mechanical properties is negligible.

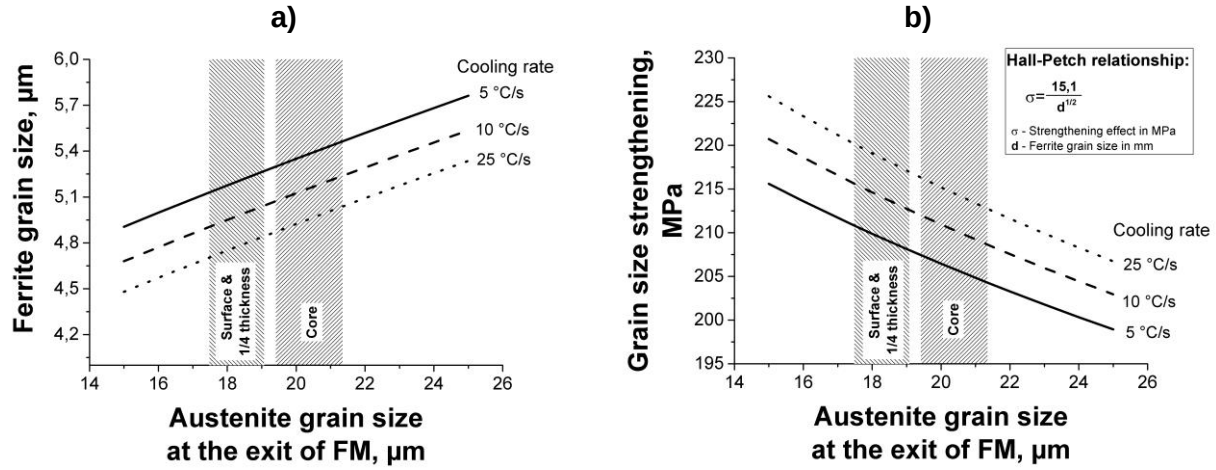

Fig. 11: a) Final ferrite grain size calculated with Eq. 13 and b) strengthening effect of ferrite grain size [23]

4 Conclusions

The product quality of HSLA steel by production using Arvedi ESP process was analysed by varying of casting parameters in a simulation of grain evolution during casting and rolling steps. The influence of casting speed and slab thickness on various aspects such as primary and secondary microstructure evolution, temperature profile and micro-segregation was considered.

The results are showing a targeted homogeneous and fine grain structure as well as good product quality at the end of the process for all assumed production scenarios. The various casting parameters are influencing the strand and transfer bar characteristics (like austenite grain size, temperature profile, …), which are equated by further processing at the induction heater and finishing rolling.

This in fact reflects that the 2 step rolling concept, by separating into a first reduction step at the HRM, the reheating at the induction heater and the forthcoming finishing rolling at a second step, serves big advantages in product quality, compared to other concepts of continuous rolling.
The most important factor for achieving the asked mechanical properties by a given chemistry is to create the right austenite structure at the end of the finishing mill and to ensure the necessary cooling rates during austenite ferrite transition. The simulation shows the advantages given by the 2 step rolling philosophy of the Arvedi ESP process for controlling the austenite and also ferrite structure for different products. For the production of more advanced steel products, asking for a certain level of accumulated strain before cooling (e.g. pipe grades), the strand and also transfer bar thicknesses can be raised to necessary values by allowing the optimized austenite structure at the same time.
The findings of this paper are further giving the possibility to cover asked productivities of an ESP line by adjusted slab thicknesses without negative influence to the microstructural evolution. According to such learnings it is reasonable to not elevate the casting speed to extraordinary high values above certain technical limits and not to risk reduced availability and increasing down times due to operational issues.
ESP lines are dimensioned accordingly and demonstrate repeating outstanding operational results on performance, process stability and availability each annual statistic.

Disclaimer: All data of the paper are not production data of the Arvedi ESP line of Cremona, they are based on simulation calculation results.

Acknowledgment
The authors acknowledge the financial support from the Climate and Energy Fund and the Austrian Research Promotion Agency (FFG).

References
[1] Camporredondo S., J. E.; Castillejos E., A. H.; Acosta G., F. A.; Gutiérrez M., E. P.; Herrera G., M. A.: Analysis of thin-slab casting by the compact-strip process: Part I. Heat extraction and solidification. Metallurgical and Materials Transactions B, 2004, 35(3), 541-560
[2] Shin, G.; Lee, S.: Development of the High Speed Thin Slab Casting Technology of POSCO. 7th European Continuous Casting Conference, 2011, Düsseldorf, Germany
[2] Miettinen, J.; Louhenkilpi, S.; Laine, J.: IDS - Solidification Analysis Package (Version 1.3.1)
[3] Pierer, R.; Bernhard, C.: On the influence of carbon on secondary dendrite arm spacing in steel. Journal of materials science, 2008, 43 (21), 6938-6943
[4] Kozeschnik, E.: MatCalc version 5.60 (rel 1.001)
[5] Andersen, I.; Grong, O.: Analytical modelling of grain growth in metals and alloys in the presence of growing and dissolving precipitates—I. Normal grain growth. Acta Metallurgica et Materialia, 1995, 43 (7), 2673-2688
[6] Bernhard, C.; Reiter, J.; Presslinger, H.: A Model for Predicting the Austenite Grain Size at the Surface of Continuously-Cast Slabs. Metallurgical and Materials Transactions B, 2008, 39B (6), 885-895
[7] Fujii, H.; Ohashi, T.; Oda, M.; Arima, R.; Hiromoto, T.: Analysis of bulging in continuously cast slabs by the creep model. Tetsu-to-Hagane 67 (8) 1981, 1172–1179.

[8] Lamant, J.Y.: Etude du gonfiement des brames de coulee continue. Rapport final, Recherche CECA 7210 CA 306, IRSID, St.-Germain en Laye 1983
[9] Han, Z.; Cai, K.; Liu, B.: Prediction and Analysis on Formation of Internal Cracks in Continuously Cast Slabs by Mathematical Models. ISIJ International, 2001, 41(12), 1473-1480
[10] Pierer, R.: Formulation of a Hot Tearing Criterion for the Continuous Casting Process, Ph.D. Thesis, University of Leoben, 2007
[11] Miettinen, J.: Mathematical Simulation of Interdendritic Solidification of Low-Alloyed and Stainless Steels. Metallurgical and Materials Transactions A, 1992, 23A, 1155-1170
[12] Bragin, S.; Rimnac, A.; Linzer, B.; Bianchi, A.; Mantova, A.; Rizzi, A.; Bernhard C.: Arvedi ESP process – an ultimate technology connecting casting and rolling in endless mode. 9th International/6th European Rolling Conference, 2013
[13] Fernández, A. I.; Uranga, P.; López, B.; Rodriguez-Ibabe, J. M.: Dynamic recrystallization behaviour covering a wide austenite grain size range in Nb and Nb–Ti microalloyed steels, Materials Science and Engineering A, 2003, 361(1-2), 367-376
[14] LI, Q.; LIU, Z.-d.; TANG, G.-b.; TIAN, Z.-l.: Siciliano, F., Mathematical Model of Microstructure Evolution of X60 Line Pipe Steel During CSP Hot Rolling. Journal of iron and steel research international, 2010, 17 (1), 70-78
[15] Uranga, P.; Fernández, A. I.; López, B.; Rodriguez-Ibabe, J. M.: Transition between static and metadynamic recrystallization kinetics in coarse Nb microalloyed austenite, Materials Science and Engineering: A, 2003, 345(1-2), 319-327
[16] Roucoules, C.; Yue, S.; Jonas, J. J.: Effect of alloying elements on metadynamic recrystallization in HSLA steels, Metallurgical and Materials Transactions A, 1995, 26(1), 181-190
[17] Fernández, A. I.; Uranga, P.; López, B.; Rodriguez-Ibabe, J. M.: Static Recrystallization Behaviour of a Wide Range of Austenite Grain Sizes in Microalloyed Steels, ISIJ International, 2000, 40(9), 893-901
[18] Abad, R.; Fernández, A. I.; López, B.; Rodriguez-Ibabe, J. M.: Interaction between Recrystallization and Precipitation during Multipass Rolling in a Low Carbon Niobium Microalloyed Steel, ISIJ International, 2001, 41 (11), 1373-1382
[19] Hodgson, P. D.; Gibbs, R. K.: A Mathematical Model to Predict the Mechanical Properties of Hot Rolled C-Mn and Microalloyed Steels, ISIJ International, 1992, 32(12), 1329-1338
[20] Karjalainen L. P.; Maccagno, T. M.; Jonas, J. J.: Softening and Flow Stress Behaviour of Nb Microalloyed Steels during Hot Rolling Simulation, ISIJ International, 1995, 35(12), 1523-1531
[21] Bengochea, R.; López, B.; Gutierrez, I.: Influence of the Prior Austenite Microstructure on the Transformation Products Obtained for C-Mn-Nb Steels after Continuous Cooling, ISIJ International, 1999, 39(6), 583-591
[22] Gladman, T.; Dulieu, D.; McIvor, I. D.: In Structure-Property Relationships in High Strength Microalloyed Steels, New York, New York, 1977; pp 32-55
[23] Bernhard, C.; Wieser, G.; Arth, G.; Presoly, P.: A Transient 2.5D-Solidification Model at the Interface between Laboratory Experiment and the Continuous Casting Process. The 7th International Conference on Physical and Numerical Simulation of Materials Processing, June 16-19 2013, Oulu, Finland